Water-Based Synthesis and Enhanced CO_2 Capture Performance of Perfluorinated Cerium-Based Metal-Organic Frameworks with UiO-66 and MIL-140 Topology

Roberto D'Amato,[1] Anna Donnadio,[2] Mariolino Carta,[3] Claudio Sangregorio,[4] Davide Tiana,[5] Riccardo Vivani,[2] Marco Taddei,[6] Ferdinando Costantino[1]**

[1] Dipartimento di Chimica Biologia e Biotecnologia, University of Perugia, Via Elce di Sotto 8, 06123 Perugia, Italy. Email: ferdinando.costantino@unipg.it

[2] Dipartimento di Scienze Farmaceutiche, University of Perugia, Via del Liceo 1, 06123 Perugia, Italy

[3] Department of Chemistry, Swansea University, Singleton Park, Sketty, Swansea, SA2 8PP, United Kingdom

[4] ICCOM-CNR, Via Madonna del Piano 10, -50019, Sesto Fiorentino, Firenze, Italy

[5] School of Chemistry, University College Cork, College Road, Cork, Ireland

[6] Energy Safety Research Institute, Swansea University, Fabian Way, Swansea, SA1 8EN, United Kingdom. Email: marco.taddei@swansea.ac.uk

KEYWORDS

Porous materials • metal-organic frameworks • green synthesis • gas separations • carbon dioxide capture

ABSTRACT

Reaction of cerium ammonium nitrate and tetrafluoroterephthalic acid in water afforded two new metal-organic frameworks with UiO-66 [F4_UiO-66(Ce)] and MIL-140 [F4_MIL-140A(Ce)] topologies. The two compounds can be obtained in the same experimental conditions, just by varying the amount of acetic acid used as crystallization modulator in the synthesis. Both F4_UiO-66(Ce) and F4_MIL-140A(Ce) feature pores with size < 8 Å, which classifies them as ultramicroporous. Combination of X-ray photoelectron spectroscopy and magnetic susceptibility measurements revealed that both compounds contain a small amount of Ce(III), which is preferentially accumulated near the surface of the crystallites. The CO_2 sorption properties of F4_UiO-66(Ce) and F4_MIL-140A(Ce) were investigated, finding that they perform better than their Zr-based analogues. F4_MIL-140A(Ce) displays an unusual S-shaped isotherm with steep uptake increase at pressure < 0.2 bar at 298 K. This makes F4_MIL-140A(Ce) exceptionally selective for CO_2 over N_2: the calculated selectivity, according to the ideal adsorbed solution theory for a 0.15:0.85 mixture at 1 bar and 293 K, is higher than 1900, amongst the highest ever reported for metal-organic frameworks. The calculated isosteric heat of CO_2 adsorption is in the range of 38-40 kJ mol^{-1}, indicating a strong physisorptive character.

Introduction

Two decades after its inception, the field of metal-organic frameworks (MOFs) is transitioning towards commercial applications.[1-3] This transition has been driving the development of synthetic methods able to produce MOFs on a large scale at a competitive cost.[4-6] At the same time, considerable interest in making such synthetic methods "greener" has been growing.[7] MOFs are often synthesised employing harmful and expensive organic solvents both as reaction media and during workup procedures,[8] therefore it is highly desirable to shift to more sustainable solvents, e.g. water[7] or dihydrolevoglucosenone (cyrene),[9] or to solvent-free synthesis, e.g. mechanochemical synthesis.[10-12] Water-based synthesis has recently been explored for Zr-based MOFs.[13-16] These MOFs have attracted considerable interest for their high thermal and hydrolytical stability, which makes them appealing for applications in real-life settings.[17] Notably, use of water as a solvent has also led to the discovery of new structural archetypes for Zr-based MOFs.[14-16] Isostructural materials to Zr-based MOFs were recently prepared employing other tetravalent species, such as Hf,[18-19] Ce,[20-24] U[25-26] and Th.[27] Ce-based MOFs have been extensively developed and a wide range of topologies based on the hexanuclear $Ce_6O_4(OH)_4(COO)_{12}$ clusters have been reported. This has primarily been pushed by the interest in taking advantage of the redox properties of Ce(IV), especially for application in catalysis.[28] These materials have only been synthesised in the presence of *N*,*N*-dimethylformamide (DMF) as a solvent so far.

Fluorinated and perfluorinated MOFs are attracting growing attention, especially for application in CO_2 capture in the presence of water, since the presence of highly polar fluorine atoms in the pores can enhance affinity for the quadrupolar CO_2 molecule, while making the framework hydrophobic.[29] A family of isostructural, hydrolytically stable and fluorinated MOFs with square

channels were recently reported, displaying the highest CO_2 physisorption capacity for trace removal and direct air capture (400 ppm, 298 K) ever reported for MOFs.[30-32]A solvent-assisted ligand incorporation (SALI) approach was also used to introduce perfluorinated alkyl chains of various lengths in the mesoporous Zr-based NU-1000, thus improving its affinity for CO_2.[33] Tetrafluoroterephthalic acid (H_2TFBDC) is a common building block for the construction of perfluorinated coordination polymers and MOFs,[29] thanks to its commercial availability. The structural analogies between H_2TFBDC and terepththalic acid (H_2BDC) could lead to assume that the preparation of perfluorinated isoreticular versions of the most common MOF topologies based on H_2BDC, such as MOF-5, UiO-66, MIL-53, MIL-101, MIL-88, should be straightforward, but so far only UiO-66(Zr) has been reported.[15] However, while water-based synthesis of MOFs containing H_2BDC is made tricky by its very low solubility, H_2TFBDC is soluble in water, probably thanks to its higher acidity (pKa: 3.32, 4.56 for H_2BDC; 1.18, 2.49 for H_2TFBDC; calculated using the online tool *Chemicalize*), and therefore attractive for greener synthetic protocols. Herein, we report on the water-based synthesis and CO_2 sorption properties of two Ce-based MOFs, having MIL-140 and UiO-66 topology, containing H_2TFBDC as a linker.

Experimental Section

Chemicals

Tetrafluoroterephtalic acid (H_2TFBDC), cerium ammonium nitrate (CAN) and acetic acid (99.5%) were purchased from Sigma-Aldrich.

Synthetic procedures

$CeO(TFBDC)\cdot H_2O$ [F4_MIL-140A(Ce)]

548 mg (1mmol) of cerium ammonium nitrate [$(NH_4)_2Ce(NO_3)_6$), CAN] and 238 mg (1 mmol) of tetrafluoroterephthalic acid (H_2TFBDC) were dissolved in 50 ml of deionized (DI) water in a round bottom flask. The solution was heated to 110 °C under stirring and refluxed for 24 h. The obtained yellow solid was collected and washed three times with DI water and once with acetone. The solid was then dried in oven at 80 °C for 24 h. Yield: 73% (calculated on the basis of Ce).

Elemental analysis: C = 22.7% exp. (23.4% calc.), H = 0.76% exp. (0.49% calc.)

$CeO_{0.67}(OH)_{0.67}(TFBDC)\cdot 3H_2O$ [F4_UiO-66(Ce)]

548 mg (1 mmol) of CAN, 238 mg (1 mmol) of H_2TFBDC and 6 mL (100 mmol) of acetic acid were dissolved in 45 ml of DI water in a round bottom flask. The solution was heated to 110 °C under stirring and refluxed for 24 h. The obtained yellow solid was collected and washed three times with DI water and once with acetone. The solid was then dried in oven at 80 °C for 24 h. Yield: 66% (calculated on the basis of Ce).

Elemental analysis: C = 23.5% exp. (22.6% calc.), H = 2.19% exp. (1.57% calc.)

Analytical procedures

Powder X-Ray Diffraction (PXRD). PXRD patterns were collected in reflection geometry with a 40 s $step^{-1}$ counting time and with a step size of 0.016° 2θ on a PANalytical X'PERT PRO diffractometer, PW3050 goniometer, equipped with an X'Celerator detector by using the Cu Kα radiation. The long fine focus (LFF) ceramic tube operated at 40 kV and 40 mA. The pattern

used for the Rietveld refinement of F4_UiO-66(Ce) was collected at 120 °C using a custom-made peltier-equipped sample holder. The same apparatus was used to collect the pattern of F4_MIL-140A(Ce) at 160 °C. The patterns of the compounds after CO_2 adsorption-desorption cyclesand of the ground pellets were collected in reflection geometry in the 4-40° 2θ range with a Bruker D8 Avance diffractometer and equipped with a LYNXEYE XE detector, using the Cu Kα radiation. The X-ray tube was operated at 40 kV and 40 mA.

Thermogravimetric analysis (TGA). TGA was performed using a Netzsch STA490C thermoanalyzer under a 20 mL min^{-1} air flux with a heating rate of 10 °C min^{-1}. For F4_UiO-66(Ce) analysis was also performed under N_2, with the same flux and heating rate.

Attenuated Total Reflectance Fourier transform infrared (ATR FT-IR). ATR FT-IR spectra were collected with a Bruker TENSOR27 spectrophotometer equipped with a globar source, a high-throughput patented RockSolid cube corner interferometer, a deuterated L-alanine tryglycine sulfate detector, and a KBr beam splitter. Transmission spectra were collected at room temperature in the 300-5000 cm^{-1} range. Each spectrum was the average of 30 scans, measured with a resolution of 2 cm^{-1}.

X-ray photoelectron spectroscopy (XPS). XPS spectra were recorded using a Kratos Axis Supra system employing a monochromated Al-Kα X-ray source; for these measurements, the powders were compressed using a two-tonne press into a circular pellet of 5 mm diameter and mounted on conductive copper tape. To maximise electrical contact between the sample plate and the pellet surface, copper clips were screwed in place over a portion of each pellet, leaving the remainder exposed for measurement. Ce core level peaks were measured using pass energy 20 eV, dwell time 1000 ms and step size 50 meV, and averaging over three sweeps. All XPS measurements

were performed over a rectangular area of 700 x 300 μm. Surface charge compensation during the XPS measurements was achieved using a charge neutraliser operating at a charge balance potential of 3.3 V, filament bias 1.0 V and filament current 0.4 A. The spectra were "carbon-corrected", with the binding energy values of each shifted by the value required to reference the C 1s peak to 284.8 eV, the accepted value for the predominant sp^3 carbon environments of adventitious organic contaminants.[34] Each core level peak was deconvoluted using Gaussian-Lorentzian product functions with 30% Lorentzian character, while the contribution of the secondary electron background was modelled using a Shirley-type function. The relative areas of the two components of each doublet were constrained following consideration of spin population statistics, and the requisite spin-orbit splitting was also imposed accordingly. The full widths at half maximum of components within a particular peak were constrained to be equal.

Magnetic measurements. Magnetic susceptibilities were measured on polycrystalline powders with a QD MPMS Squid magnetometer. Data were corrected for the contribution of the sample holder, which was separately measured, and for the underlying diamagnetism of the sample, evaluated from Pascal's constant.

Gas sorption analysis. N_2 and CO_2 sorption isotherms were measured on a Quantachrome Nova 2000e analyser at 77 K (N_2), 273 K (CO_2), 293 K (N_2, CO_2) and 313 K (CO_2). The samples (about 100 mg) were activated overnight under vacuum at 120 °C prior to analysis. Using the N_2 isotherms at 77 K, BET surface areas were calculated in the 0.015-0.021 P/P_0 range for F4_UiO-66(Ce) and in the 0.013-0.045 P/P_0 range for F4_MIL-140A(Ce). Total pore volume was determined at P/P_0 0.52 for both compounds. Using the CO_2 isotherms at 273 K, pore size distributions were determined with the non local density functional theory (NLDFT) method implemented in the Quantachrome NovaWin software. CO_2 isotherms for F4_UiO-66(Ce) were

fitted to the Single Site Langmuir-Freundlich model at 273 K and 293 K, whereas a simple linear fit was found to be best at 313 K (common models for adsorption isotherms resulted in overparametrization). CO_2 isotherms for F4_MIL-140A(Ce) were fitted to the Dual Site Langmuir-Freundlich model. N_2 isotherms at 293 K for both compounds were fitted to the Single Site Langmuir-Freundlich model. The isosteric heat of CO_2 adsorption (Q_{st}) was calculated by using the linear version of the Clausius-Clapeyron equation in the loading range 0.05-1.0 mmol g^{-1}. Ideal adsorbed solution theory (IAST) CO_2/N_2 selectivity for a 0.15:0.85 CO_2/N_2 mixture in the pressure range 0.1-1.0 bar was calculated using the simulated mixed gas isotherms obtained from the software *IAST++*.[35] To test the recyclability of the sorbents, three CO_2 adsorption-desorption cycles were run at 273 K for each MOF, with activation at 120 °C for 4 hours in between consecutive cycles.

Computational methodology

The theoretical surface and accessible volume were calculated using the code Zeo++, which is the standard code used for calculating accessible internal surfaces and volumes of porous materials.[36-37] After having performed a Voronoi decomposition of the space, the accessible internal surface and volume are calculated with a Monte Carlo simulation using a probe of radius *r* to simulate the guest molecule inside of the pore. Despite producing good result, it should be note that the following limitations are present for this approximation: 1. the guest molecule is assumed to be a perfect sphere, which is not the case of N_2; 2. the simulations are static, i.e., vibration due to thermal motions and crystal structure changes upon adsorption (e.g. pore swelling or ligand rotation) are not considered. As demonstrated by Ongari et al., this can lead to discrepancy when dealing with narrow channels or small pores.[37]

Results and Discussion

The MOF of formula $CeO(F_4\text{-}BDC)\cdot H_2O$ [hereafter F4_MIL-140A(Ce)] was synthesised by refluxing a water solution of cerium(IV) ammonium nitrate (CAN) and H_2TFBDC at 110 °C for 24 h. Simple addition of 100 equivalents of acetic acid (AcOH) as a crystallisation modulator to the synthetic mixture afforded $Ce_6O_4(OH)_4(F_4\text{-}BDC)_6\cdot 18H_2O$ (hereafter F4_UiO-66(Ce)]. Using lower amounts of AcOH led to the formation of mixed phases (Figure S1). A certain amount of AcOH was found necessary to aid the formation of discrete hexanuclear $Ce_6O_4(OH)_4(COO)_{12}$ clusters for the UiO-66 structure, slowing down the crystallisation rate and preventing formation of the more condensed and extended inorganic connectivity of the MIL-140 structure. Interestingly, in the UiO-66(Zr)/MIL-140A(Zr) system, the UiO-66 topology is the kinetic product and the MIL-140 topology is the thermodynamic one,[38] whereas in the case of F4_UiO-66(Ce) and F4_MIL-140A(Ce) the situation is apparently reverted and the MIL-140 structure is the kinetically favoured phase. The phase-pure solids were crystalline enough to allow us to determine the crystal structures and perform Rietveld refinement on the powder X-ray diffraction (PXRD) data (see SI for details of structure solution and refinement procedures, Table S1 Figures S2-S3).

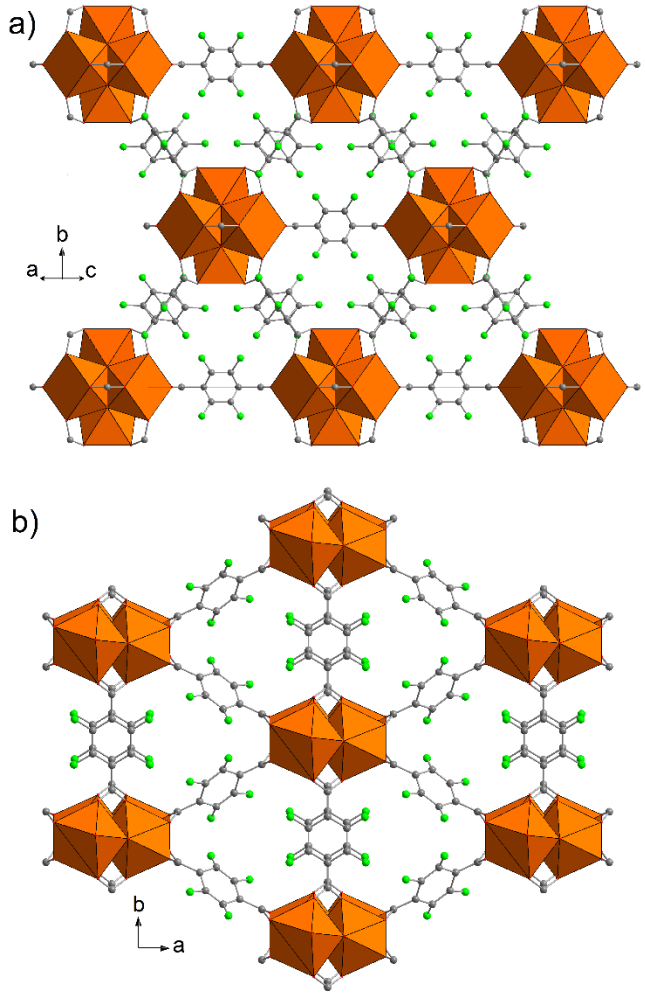

Figure 1. The crystal structures of F4_UiO-66(Ce) (a) and F4_MIL140A(Ce) (b). Colour code: Ce, orange; O, red; C, grey; F, green.

F4_UiO-66(Ce) displays the well-known face centered cubic structure of UiO-66 type (Figure 1a),[39] featuring twelve-connected hexanuclear $Ce_6O_4(OH)_4(COO)_{12}$ clusters, with a slightly larger lattice parameter [21.541(2) Å] than its non-perfluorinated analogue [21.4727(3) Å].[21] The perfluorinated phenyl rings lie outside the plane of the carboxylate groups and are disordered over two symmetrically related positions (Figure S4). This is due to the steric repulsion between the fluorine atoms on the ring and the carboxylic groups and is commonly observed in compounds containing the H_2TFBDC linker, including F4_UiO-66(Zr).[15] Brunauer-Emmett-

Teller (BET) analysis of the N_2 adsorption isotherm collected at 77 K gave surface area of 641 $m^2 g^{-1}$ and pore volume of 0.26 $cm^3 g^{-1}$ (Figure S5). These values are considerably lower than those measured for the analogous UiO-66(Ce) (1282 $m^2 g^{-1}$ and 0.50 $cm^3 g^{-1}$, respectively)[21] and similar to those of the Zr-based analogue F4_UiO-66(Zr) (640-690 $m^2 g^{-1}$ and 0.24 $cm^3 g^{-1}$, respectively).[15, 40] Theoretical surface area and pore volume were determined using 500000 Monte Carlo sampling and a probe with a radius of 1.8 Å, similar to N_2. The accessible internal surface was found to be 734 $m^2 g^{-1}$, while the accessible internal volume 0.27 $cm^3 g^{-1}$ .The small difference can be attributed to the fact that the calculations does not take into account any type of vibrations which, considering the aromatic rings are disordered, are likely to be present also a 77 K. These number suggest that F4_UiO-66(Ce) is most likely a defect-free phase. Pore size distribution (PSD), as determined applying the non local density functional theory (NLDFT) method to the CO_2 adsorption isotherm measured at 273 K, displays a maximum around 6 Å diameter. ^{1}H nuclear magnetic resonance (NMR) analysis of the compound hydrolyzed in 0.1 M NaOH revealed the absence of the AcOH modulator, suggesting again that F4_UiO-66(Ce) is non-defective. This is further corroborated by the good agreement between the experimental and calculated C and H content obtained from elemental analysis. F4_UiO-66(Ce) is thermally stable up to about 280 °C (Figure S6), comparable to other previously reported Ce-based MOFs.[21] It is worth to note that F4_UiO-66(Ce) undergoes explosive decomposition, which leads to ejection of powder from the sample holder, as evidenced by the vertical loss in the TGA curve of this MOF, both in air and under nitrogen (Figures S6-7). This phenomenon prevented us from extracting additional information regarding the defectivity of the framework, because of the impossibility to distinguish between the weight loss due to thermal decomposition of the framework and the weight loss due to loss of powder from the sample holder. FT-IR analysis

(Figure S8) shows that most of the bands observed for F4_UiO-66(Ce) match with those of the H_2TFBDC linker.

F4_MIL-140A(Ce) has the same crystal structure of MIL-140A(Zr), first reported in 2012 (Figure 1b).[38] To the best of our knowledge, F4_MIL-140A(Ce) is the first member of the MIL-140 family to be 1. based on Ce as the metal ion, 2. based on H_2TFBDC as the organic linker, 3. synthesised in water. The unit cell of F4_MIL-140A(Ce) is larger than that of MIL-140A(Zr), as a consequence of the larger ionic radius of Ce(IV) (ranging between 0.87 and 0.97 Å for coordination number VI and VIII, respectively)[41] with respect to Zr(IV) (ranging between 0.72 and 0.84 Å for coordination number VI and VIII, respectively).[41] The structure of F4-MIL-140A(Ce) is composed of 1D inorganic building units (IBUs) running along the *c* axis and built from the connection of edge-sharing CeO_7 units, carboxylate groups and μ_3-oxide bridges. These IBUs are connected to each other, along the *a* and the *b* axes, through the $TFBDC^{2-}$ moieties, thus designing 1D triangular channels with aperture of approximately 4.8 x 5.8 Å, measured from the atomic centres (Figure S9). Similar to F4_UiO-66(Ce), the perfluorinated phenyl rings in F4_MIL-140A(Ce) lie outside of the plane of the carboxylates (Figure S10). However, due to the lower symmetry of F4_MIL-140A(Ce), no disorder is observed. The unit cell of F4_MIL-140A(Ce) contains one water molecule per Ce atom, with a Ce-O distance of 2.94 Å, which suggests that a weak coordinative interaction could exist between them (Figure S11). The effect of dehydration on the structure of F4_MIL-140A(Ce) was evaluated by collecting a PXRD pattern on the compound heated to 160 °C (Figure S12). Pawley refinement shows that symmetry was retained and the unit cell volume only shrunk by 1% (Table S1, Figure S13), thus suggesting that no major structural rearrangement takes place upon removal of water from the coordination sphere of the Ce atoms. BET analysis of the N_2 adsorption isotherm collected at 77

K gave surface area of 320 $m^2 g^{-1}$ and pore volume of 0.11 $cm^3 g^{-1}$ (Figure S5). These values are lower than those measured for the prototypical MIL-140A(Zr) (415 $m^2 g^{-1}$ and 0.18 $cm^3 g^{-1}$, respectively).[38] In this case, using a probe with radius of 1.8 Å, Zeo++ does not find any channel. This is clearly an artefact due to the limitation of the algorithm when dealing with small pores. As done in the original article, when the probe was readjusted at 1.6 Å and 1.4 Å for screening of zeolites internal surface and volume,[36] the size of the probe was decreased until the algorithm correctly reproduced the channels existing in the crystal structure (i.e., r = 1.3 Å). The accessible internal surface was then calculated as 332 $m^2 g^{-1}$, whilst the accessible volume was found to be 0.10 $m^2 g^{-1}$, both in excellent agreement with the experimental ones. PSD, as determined applying the NLDFT method to the CO_2 adsorption isotherm measured at 273 K, displays a single peak around 4.2 Å diameter, in line with what expected from the size of the channels observed in the crystal structure. F4_MIL-140A(Ce) is thermally stable up to about 300 °C (Figure S6), slightly more than F4_UiO-66(Ce), but considerably less than variously functionalised Zr-based MIL-140A MOFs, which can reach up to about 500 °C.[38] No explosive decomposition was observed for F4_MIL-140A(Ce). The reason for this different behaviour is not obvious and is likely to be related to the different structural arrangement of the two MOFs. This allowed us to compare the expected and experimental weight losses for F4_MIL-140A(Ce): the expected weight loss upon loss of water molecules at 160 °C is 4.4%, in good agreement with the experimental loss of 4.8%. The expected final weight loss upon decomposition of the framework and formation of CeO_2 at 1200 °C is 58.0%, in good agreement with the experimental loss of 58.5%. This, in combination with the good agreement between the experimental and calculated C and H content obtained from elemental analysis, proves that F4_MIL-140A(Ce) does not contain defects. The FT-IR spectrum of F4_MIL-140A(Ce) is very similar to that of

F4_UiO-66(Ce) (Figure S8), the main difference being the absence of the broad band due to hydrogen-bonded water.

Ce(IV) is a powerful oxidant species that can easily lose one electron to yield Ce(III). The standard reduction potential for the Ce(IV)/Ce(III) pair is +1.75 V, higher than the standard potential for water oxidation (+1.23 V).[42] This means that, during a water-based synthesis at reflux temperature, part of the original Ce(IV) could be reduced to Ce(III) and that some Ce(III) could be incorporated in the resulting MOF. It was recently reported that hexanuclear Ce(IV) clusters decorated with glycine and nitrate anions display a reduction potential of +0.60 V vs Ag/AgCl in the presence of 0.1 M HNO_3, corresponding to a standard reduction potential of about +0.80 V, not sufficient for water oxidation.[43] This would suggest that, once the clusters are formed, they should not be able to oxidise water and, as a consequence, no reduction to Ce(III) should occur. However, coordination of Ce by a perfluorinated linker could impact on its redox behavior. To the best of our knowledge, there are no studies investigating the effect of ligand electronic effects on the redox properties of Ce coordination compounds. However, Lanznaster et al.[44] have studied the redox behavior of Fe complexes with the N,N‘-bis(2-hydroxybenzyl)-N,N‘-bis(pyridin-2-ylmethyl)ethylenediamine containing electron-donating and -withdrawing groups (Me, Br, NO_2) in the 5-position of the phenol rings. They found that the presence of electron-withdrawing nitro groups in the ligand tends to stabilise Fe(II), whereas electron-donating methyl groups tend to stabilise Fe(III). This would suggest that a perfluorinated linker, which has a marked electron-withdrawing character, could favour the presence of Ce(III) species in these MOFs. For this reason, we set out to determine the oxidation state of Ce in F4_UiO-66(Ce) and F4_MIL-140A(Ce). Stock and co-workers have used X-ray absorption near-edge spectroscopy (XANES), finding no evidence of Ce(III) in several Ce-based MOFs.[20-21] While XANES is a

powerful method that can provide direct information about oxidation states, it is a synchrotron-based technique, which makes it not readily accessible for everyone. More recently, Dalapati et al.[24] employed X-ray photoelectron spectroscopy (XPS), observing 23.6% of Ce(III) in a Ce-MOF with UiO-66 topology. However, XPS is a surface sensitive technique, meaning that no information about the bulk is obtained. Here, we have employed a combination of XPS and magnetic susceptibility measurements, which can provide complementary quantitative information about the surface and the bulk, respectively.

The region between 875 and 920 eV binding energy of the XPS spectra (Figure 2a-b), where the Ce 3d core level peaks appear, was analysed to investigate the oxidation state of Ce. The six peaks at 882.3, 888.2, 898.1, 900.8, 906.7 and 916.6 eV correspond to Ce(IV), while the four peaks at 880.5, 885.0, 899.0 and 903.4 eV correspond to Ce(III) (see Table S2 for details on peak assignments and areas).[45-46] The analysis reveals the presence of significant quantities of Ce(III): 69.9% in F4_UiO-66(Ce) and 42.9% in F4_MIL-140A(Ce). In order to ensure that sample preparation did not lead to amorphisation, PXRD analysis of the ground pellets used for XPS analysis was carried out. This shows that the diffraction peaks of F4_UiO-66(Ce) suffers from peak broadening upon compression (Figure S14), whereas F4_MIL-140A(Ce does not show major loss of crystallinity (Figure S15), in agreement with the higher mechanical stability reported for MIL-140 type frameworks.[38] Magnetic susceptibility data for F4_UiO-66(Ce) and F4_MIL-140A(Ce) (Figure 2c) reveal for both samples the presence of a weak paramagnetic signal, which can be attributed to a small amount of Ce(III). From the room temperature valued of the χT product (inset of Figure 2c), the percentage of Ce^{III} was estimated as 7 ± 1 % and 5 ± 1 % for F4_UiO-66(Ce) and F4_MIL140A, respectively. The evaluation was performed by considering that in the literature most of mononuclear compounds of Ce^{3+} are reported to have

χT values in the range 0.55-0.75 cm^3 K mol^{-1}.[47-48] These results suggest that the moderate amount of Ce(III) present in both materials is preferentially located on the external surface of the crystallites. We speculate that this Ce(III) accumulation near the external surface can be due to water oxidation occurring at the solid/liquid interface during the synthetic process. It seems clear that this aspect deserves further deep investigation and will be addressed in a future work.

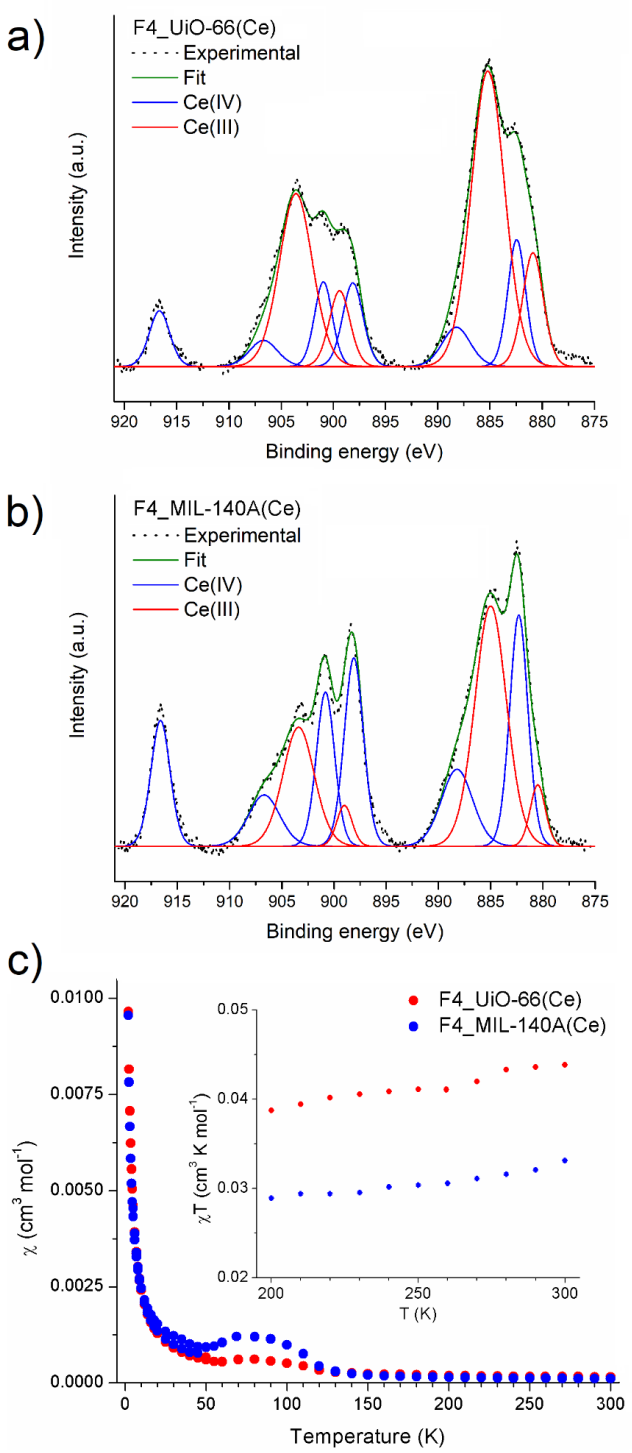

Figure 2. Deconvoluted XPS spectra of F4_UiO-66(Ce) (a) and F4_MIL-140A(Ce) (b) in the Ce core level region. Ce(IV) components are represented in blue, Ce(III) components are represented in red, the resulting fitting curve is represented in olive. Thermal dependence of

magnetic susceptibility (c) for F4_UiO-66(Ce) (red symbols) and F4_MIL140A(Ce) (blue symbols) measured with an applied field $\mu_0 H$ = 1.0 kOe (up to 50 K) and 10 kOe (from 30 K). In the inset the corresponding χT values in the high temperature range (200-300 K) are reported.

The CO_2 sorption properties of F4_UiO-66(Ce) and F4_MIL-140A(Ce) were investigated collecting adsorption isotherms up to 1 bar at 273, 293 and 313 K (Figure 3).

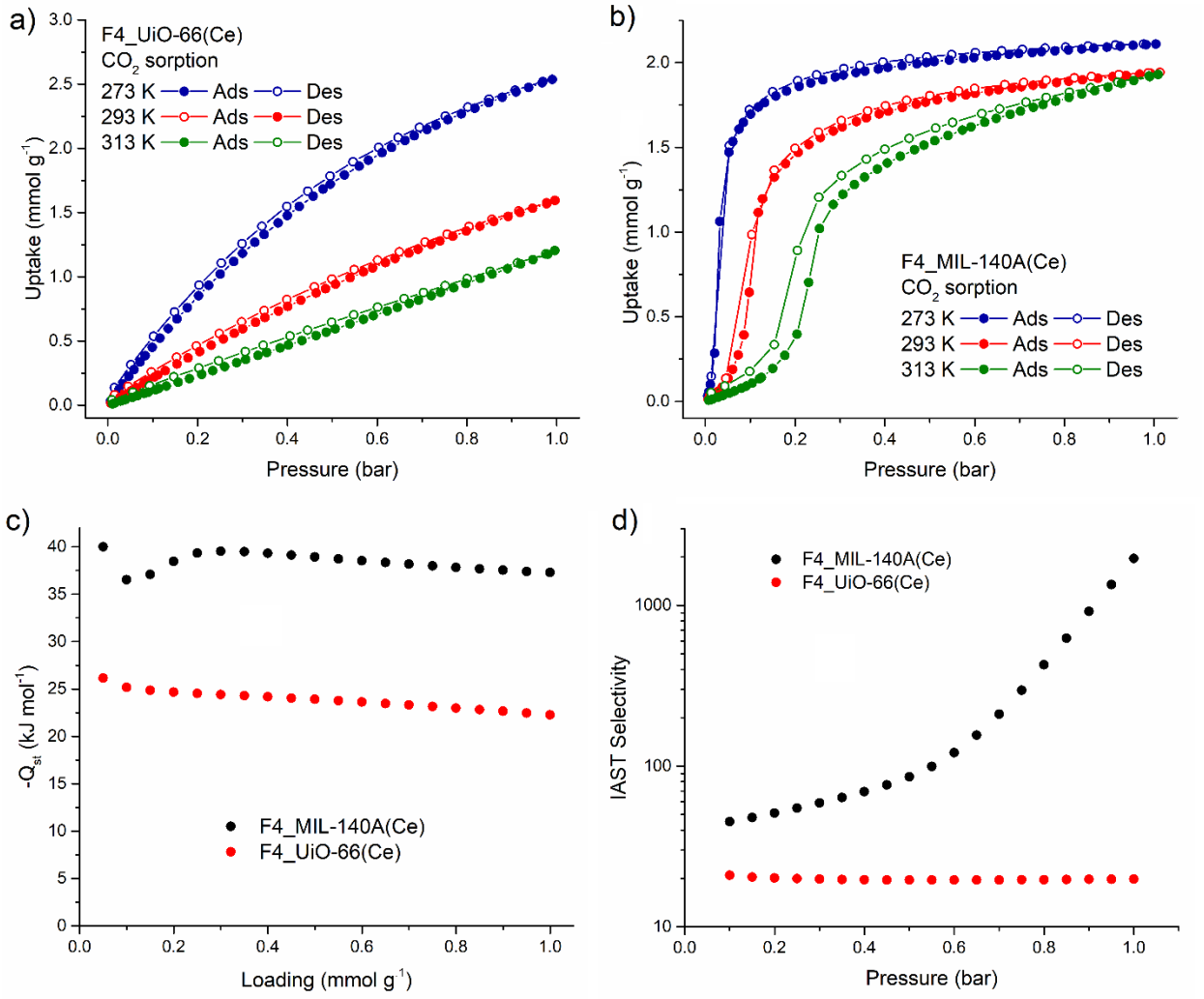

Figure 3. CO_2 adsorption (filled circles) and desorption (empty circles) isotherms collected at 273 K (blue), 293 K (red) and 313 K (green) for F4_UiO-66(Ce) (a) and F4_MIL-140A(Ce) (b). Plot of the isosteric heat of CO_2 adsorption as a function of loading (c) and IAST selectivity as a

function of total pressure for a 0.15:0.85 CO_2/N_2 mixture at 298 K (d) for F4_UiO-66(Ce) (red circles) and F4_MIL-140A(Ce) (black circles).

F4_UiO-66(Ce) displays slightly improved CO_2 sorption properties, if compared to its Zr-based analogue. The uptake at 1 bar and 273 K increases from 1.9 mmol g^{-1} for F4_UiO-66(Zr)[40] to 2.5 mmol g^{-1} for F4_UiO-66(Ce), corresponding to about 11.0 wt% (Figure 3a, Figure S16). When compared to other Ce-based MOFs with the same UiO-66 topology (Table S3),[49-51] F4_UiO-66(Ce) displays average performance. Recyclability of F4_UiO-66(Ce) was tested by running three CO_2 adsorption-desorption cycles at 273 K, finding that the isotherms are perfectly reproducible (Figure S17) and that no loss of crystallinity occurs (Figure S14). The CO_2/N_2 selectivity calculated according to the ideal adsorbed solution theory (IAST)[35] model for a 0.15:0.85 mixture at 1 bar increases from 6 for F4_UiO-66(Zr) (at 298 K)[40] to 20 for F4_UiO-66(Ce) (at 293 K, Figure 3d, Figure S18). The improvement can be partially explained by the slightly higher value of isosteric heat of CO_2 adsorption (Q_{st}, calculated using the Clausius-Clapeyron equation) for F4_UiO-66(Ce) (comprised between 22 and 25 kJ mol^{-1} at loading < 1 mmol g^{-1}, Figure 3c) if compared to that of the Zr-based analogue (22.4 kJ mol^{-1}).[40]

F4_MIL-140A(Ce) shows a rather unusual and much more interesting S-shape of the CO_2 sorption isotherm (Figure 3b, Figure S19), and deserves to be discussed more in detail. Saturation of the pores of F4_MIL-140A(Ce) with CO_2 occurs over a small range of pressure and the inflection point in the isotherm is shifted to higher pressure as the temperature increases (0.03 bar at 273 K, 0.10 bar at 293 K, 0.23 bar at 313 K; Figure S20). This type of behavior is typical of so-called "phase-change" adsorbents and is usually attributed to very specific interactions of the quadrupolar CO_2 molecule with the sorbent surface. It was recently observed for the amine-appended MOF mmen-M_2(dobpdc) (with M = Mg^{2+}, Mn^{2+}, Fe^{2+}, Co^{2+}, Zn^{2+}), where CO_2 is

cooperatively inserted into metal-amine bonds, forming a carbamate species and leading to a rearrangement in the metal coordination sphere.[52] Given the absence of amine groups in F4_MIL-140A(Ce), we can exclude this specific adsorption mechanism. Similar shape is also displayed by IRMOF-1, but it only becomes visible at temperature < 233 K,[53] much lower than in the case of F4_MIL-140A(Ce). The absence of significant hysteresis upon desorption of CO_2 (Figure 3b) suggests that a proper gate-opening process could probably be excluded.[54-55] The total uptake of F4_MIL-140A(Ce) at 1 bar and 293 K is 1.9 mmol g^{-1}, corresponding to 8.4 wt%, (Figure 3b) and is the highest reported so far for MOFs having MIL-140 topology.[56] Such uptake is moderate, if compared with other MOFs,[57] and is mostly due to the small pore volume of F4_MIL-140A(Ce). However, the non-hysteretic S-shaped isotherm potentially allows for a temperature-swing adsorption process with high working capacity and little energy penalty, which is of high practical interest.[52] Recyclability of F4_MIL-140A(Ce) was tested by running three CO_2 adsorption-desorption cycles at 273 K, finding that the isotherms are perfectly reproducible (Figure S21) and that no loss of crystallinity occurs (Figure S15). The most striking feature of F4_MIL-140A(Ce) is its exceptional CO_2/N_2 IAST selectivity of 1962 (0.15:0.85 mixture at 1 bar and 293 K, Figure 3d, Figure S22), comparable to that of the fluorinated SIFSIX-3-Zn (1818, for a 0.15:0.85 mixture at 1 bar and 298 K)[30] and ranking amongst the highest ever reported for MOFs.[57] The value of Q_{st} stays relatively constant at about 40 kJ mol^{-1} at loading < 1 mmol g^{-1} (Figure 3c), slightly lower than that of SIFSIX-3-Zn (45 kJ mol^{-1}). This value suggests that there is a favorable interaction between the adsorbate and the surface, but no formation of strong chemical bonds is involved. Similar to SIFSIX-3-Zn, F4_MIL-140A(Ce) features small channel-like pores lined with highly polar F atoms, which most likely represent an ideal combination to create favorable environment to selectively adsorb CO_2 over N_2. In

addition, a weak coordinative interaction of CO_2 with the metal atoms could be involved, similar to that existing between water and the metal atoms in the as synthesized material.

Conclusions

We have presented a very simple, water-based method to synthesise two new perfluorinated Ce-based MOFs having UiO-66 and MIL-140 topology. The crystal structures of the two materials were determined and refined using PXRD data. XPS and magnetic susceptibility measurements revealed that both compounds contain higher amount of Ce(III), preferentially located near the external surface of the crystallites, than previously reported Ce-based MOFs. The two compounds display enhanced CO_2 capture performance, in terms of uptake and selectivity over N_2, if compared to their Zr-based analogues. The S-shape CO_2 isotherm observed for F4_MIL-140A(Ce) is responsible for its exceptional selectivity over N_2 and can be advantageous for achieving high working capacity and low energy penalty in a temperature-swing adsorption process. Future efforts will be devoted to better understanding the origin of the unusual CO_2 sorption behaviour of F4_MIL-140A(Ce),to investigating the crystallisation mechanism of the F4_UiO-66(Ce)/ F4_MIL-140A(Ce) polymorphic system in water and to studying the redox behaviour of Ce in these systems.

ASSOCIATED CONTENT

Supporting Information.

The following files are available free of charge:

- Supporting information file (PDF).

- Crystallographic information file (cif) for F4_UiO-66(Ce) and F4_MIL-140A(Ce) (cif). This data can be obtained free of charge from the Cambridge Crystallographic Data Centre under

entries CCDC-1855704 and CCDC-1855705 via www.ccdc.cam.ac.uk/data_request/cif

- Input file used for Rietveld refinement of F4_UiO-66(Ce) in TOPAS (txt).

AUTHOR INFORMATION

Corresponding Authors

* marco.taddei@swansea.ac.uk; ferdinando.costantino@unipg.it

Funding Sources

M.T. is supported by funding from the European Union's Horizon 2020 research and innovation programme under the Marie Skłodowska-Curie grant agreement No 663830. The authors wish to acknowledge the Irish Centre for High-End Computing (ICHEC) for the provision of computational facilities.

ACKNOWLEDGMENT

The authors thank Dr Daniel R. Jones (Swansea University) for collecting XPS spectra and Prof Paola Sassi (University of Perugia) for collecting FTIR spectra. The authors thank Prof Serena Margadonna (Swansea University) for providing access to the Bruker powder X-ray diffractometer. The authors thank Daniele Ongari (EPFL Valais) for fruitful discussion.

REFERENCES

1. Frameworks for commercial success. *Nature Chemistry* **2016,** *8*, 987.
2. Yilmaz, B.; Trukhan, N.; Müller, U., Industrial Outlook on Zeolites and Metal Organic Frameworks. *Chin. J. Catal.* **2012,** *33* (1), 3-10.
3. Silva, P.; Vilela, S. M.; Tome, J. P.; Almeida Paz, F. A., Multifunctional metal-organic frameworks: from academia to industrial applications. *Chem. Soc. Rev.* **2015,** *44* (19), 6774-6803.
4. DeSantis, D.; Mason, J. A.; James, B. D.; Houchins, C.; Long, J. R.; Veenstra, M., Techno-economic Analysis of Metal–Organic Frameworks for Hydrogen and Natural Gas Storage. *Energy & Fuels* **2017,** *31* (2), 2024-2032.
5. Rubio-Martinez, M.; Avci-Camur, C.; Thornton, A. W.; Imaz, I.; Maspoch, D.; Hill, M. R., New synthetic routes towards MOF production at scale. *Chem. Soc. Rev.* **2017,** *46* (11), 3453-3480.
6. Ren, J.; Dyosiba, X.; Musyoka, N. M.; Langmi, H. W.; Mathe, M.; Liao, S., Review on the current practices and efforts towards pilot-scale production of metal-organic frameworks (MOFs). *Coord. Chem. Rev.* **2017,** *352*, 187-219.
7. Reinsch, H., "Green" Synthesis of Metal-Organic Frameworks. *Eur. J. Inorg. Chem.* **2016,** *2016* (27), 4290-4299.
8. Stock, N.; Biswas, S., Synthesis of metal-organic frameworks (MOFs): routes to various MOF topologies, morphologies, and composites. *Chem. Rev.* **2012,** *112* (2), 933-969.
9. Zhang, J.; White, G. B.; Ryan, M. D.; Hunt, A. J.; Katz, M. J., Dihydrolevoglucosenone (Cyrene) As a Green Alternative to N,N-Dimethylformamide (DMF) in MOF Synthesis. *ACS Sust. Chem. Eng.* **2016,** *4* (12), 7186-7192.
10. James, S. L.; Adams, C. J.; Bolm, C.; Braga, D.; Collier, P.; Friščić, T.; Grepioni, F.; Harris, K. D. M.; Hyett, G.; Jones, W.; Krebs, A.; Mack, J.; Maini, L.; Orpen, A. G.; Parkin, I. P.; Shearouse, W. C.; Steed, J. W.; Waddell, D. C., Mechanochemistry: opportunities for new and cleaner synthesis. *Chem. Soc. Rev.* **2012,** *41* (1), 413-447.
11. Crawford, D.; Casaban, J.; Haydon, R.; Giri, N.; McNally, T.; James, S. L., Synthesis by extrusion: continuous, large-scale preparation of MOFs using little or no solvent. *Chem. Sci.* **2015,** *6* (3), 1645-1649.
12. Uzarevic, K.; Wang, T. C.; Moon, S. Y.; Fidelli, A. M.; Hupp, J. T.; Farha, O. K.; Friscic, T., Mechanochemical and solvent-free assembly of zirconium-based metal-organic frameworks. *Chem. Commun.* **2016,** *52* (10), 2133-2136.
13. Zahn, G.; Schulze, H. A.; Lippke, J.; König, S.; Sazama, U.; Fröba, M.; Behrens, P., A water-born Zr-based porous coordination polymer: Modulated synthesis of Zr-fumarate MOF. *Microporous Mesoporous Mater.* **2015,** *203*, 186-194.
14. Waitschat, S.; Reinsch, H.; Stock, N., Water-based synthesis and characterisation of a new Zr-MOF with a unique inorganic building unit. *Chem. Commun.* **2016,** *52* (86), 12698-12701.
15. Reinsch, H.; Bueken, B.; Vermoortele, F.; Stassen, I.; Lieb, A.; Lillerud, K.-P.; De Vos, D., Green synthesis of zirconium-MOFs. *CrystEngComm* **2015,** *17* (22), 4070-4074.
16. Taylor, J. M.; Komatsu, T.; Dekura, S.; Otsubo, K.; Takata, M.; Kitagawa, H., The Role of a Three Dimensionally Ordered Defect Sublattice on the Acidity of a Sulfonated Metal-Organic Framework. *J. Am. Chem. Soc.* **2015,** *137* (35), 11498-11506.

17. Bai, Y.; Dou, Y.; Xie, L. H.; Rutledge, W.; Li, J. R.; Zhou, H. C., Zr-based metal-organic frameworks: design, synthesis, structure, and applications. *Chem. Soc. Rev.* **2016,** *45* (8), 2327-2367.
18. Jakobsen, S.; Gianolio, D.; Wragg, D. S.; Nilsen, M. H.; Emerich, H.; Bordiga, S.; Lamberti, C.; Olsbye, U.; Tilset, M.; Lillerud, K. P., Structural determination of a highly stable metal-organic framework with possible application to interim radioactive waste scavenging: Hf-UiO-66. *Phys. Rev. B* **2012,** *86* (12), 125429.
19. Bon, V.; Senkovskyy, V.; Senkovska, I.; Kaskel, S., Zr(IV) and Hf(IV) based metal-organic frameworks with reo-topology. *Chem. Commun.* **2012,** *48* (67), 8407-8409.
20. Rhauderwiek, T.; Heidenreich, N.; Reinsch, H.; Øien-Ødegaard, S.; Lomachenko, K. A.; Rütt, U.; Soldatov, A. V.; Lillerud, K. P.; Stock, N., Co-Ligand Dependent Formation and Phase Transformation of Four Porphyrin-Based Cerium Metal–Organic Frameworks. *Cryst. Growth Des.* **2017,** *17* (6), 3462-3474.
21. Lammert, M.; Wharmby, M. T.; Smolders, S.; Bueken, B.; Lieb, A.; Lomachenko, K. A.; Vos, D. D.; Stock, N., Cerium-based metal organic frameworks with UiO-66 architecture: synthesis, properties and redox catalytic activity. *Chem. Commun.* **2015,** *51* (63), 12578-12581.
22. Lammert, M.; Reinsch, H.; Murray, C. A.; Wharmby, M. T.; Terraschke, H.; Stock, N., Synthesis and structure of Zr(iv)- and Ce(iv)-based CAU-24 with 1,2,4,5-tetrakis(4-carboxyphenyl)benzene. *Dalton Trans.* **2016,** *45* (47), 18822-18826.
23. Lammert, M.; Glißmann, C.; Reinsch, H.; Stock, N., Synthesis and Characterization of New Ce(IV)-MOFs Exhibiting Various Framework Topologies. *Cryst. Growth Des.* **2017,** *17* (3), 1125-1131.
24. Dalapati, R.; Sakthivel, B.; Ghosalya, M. K.; Dhakshinamoorthy, A.; Biswas, S., A cerium-based metal–organic framework having inherent oxidase-like activity applicable for colorimetric sensing of biothiols and aerobic oxidation of thiols. *CrystEngComm* **2017,** *19* (39), 5915-5925.
25. Falaise, C.; Volkringer, C.; Vigier, J. F.; Henry, N.; Beaurain, A.; Loiseau, T., Three-dimensional MOF-type architectures with tetravalent uranium hexanuclear motifs (U6O8). *Chem. Eur. J.* **2013,** *19* (17), 5324-5331.
26. Falaise, C.; Volkringer, C.; Loiseau, T., Mixed Formate-Dicarboxylate Coordination Polymers with Tetravalent Uranium: Occurrence of Tetranuclear {U4O4} and Hexanuclear {U6O4(OH)4} Motifs. *Cryst. Growth Des.* **2013,** *13* (7), 3225-3231.
27. Falaise, C.; Charles, J. S.; Volkringer, C.; Loiseau, T., Thorium terephthalates coordination polymers synthesized in solvothermal DMF/H2O system. *Inorg. Chem.* **2015,** *54* (5), 2235-2242.
28. Smolders, S.; Lomachenko, K. A.; Bueken, B.; Struyf, A.; Bugaev, A. L.; Atzori, C.; Stock, N.; Lamberti, C.; Roeffaers, M. B. J.; De Vos, D. E., Unravelling the Redox-catalytic Behavior of Ce(4+) Metal-Organic Frameworks by X-ray Absorption Spectroscopy. *ChemPhysChem* **2018,** *19* (4), 373-378.
29. Noro, S.-i.; Nakamura, T., Fluorine-functionalized metal–organic frameworks and porous coordination polymers. *NPG Asia Mater.* **2017,** *9* (9), e433.
30. Nugent, P.; Belmabkhout, Y.; Burd, S. D.; Cairns, A. J.; Luebke, R.; Forrest, K.; Pham, T.; Ma, S.; Space, B.; Wojtas, L.; Eddaoudi, M.; Zaworotko, M. J., Porous materials with optimal adsorption thermodynamics and kinetics for CO2 separation. *Nature* **2013,** *495* (7439), 80-84.

31. Shekhah, O.; Belmabkhout, Y.; Chen, Z.; Guillerm, V.; Cairns, A.; Adil, K.; Eddaoudi, M., Made-to-order metal-organic frameworks for trace carbon dioxide removal and air capture. *Nat. Comm.* **2014,** *5*, 4228.
32. Bhatt, P. M.; Belmabkhout, Y.; Cadiau, A.; Adil, K.; Shekhah, O.; Shkurenko, A.; Barbour, L. J.; Eddaoudi, M., A Fine-Tuned Fluorinated MOF Addresses the Needs for Trace CO2 Removal and Air Capture Using Physisorption. *J. Am. Chem. Soc.* **2016,** *138* (29), 9301-9307.
33. Deria, P.; Mondloch, J. E.; Tylianakis, E.; Ghosh, P.; Bury, W.; Snurr, R. Q.; Hupp, J. T.; Farha, O. K., Perfluoroalkane functionalization of NU-1000 via solvent-assisted ligand incorporation: synthesis and CO2 adsorption studies. *J. Am. Chem. Soc.* **2013,** *135* (45), 16801-16804.
34. McCafferty, E.; Wightman, J. P., Determination of the concentration of surface hydroxyl groups on metal oxide films by a quantitative XPS method. *Surf. Interface Anal.* **1998,** *26* (8), 549-564.
35. Lee, S.; Lee, J. H.; Kim, J., User-friendly graphical user interface software for ideal adsorbed solution theory calculations. *Kor. J. Chem. Eng.* **2017,** *35* (1), 214-221.
36. Willems, T. F.; Rycroft, C. H.; Kazi, M.; Meza, J. C.; Haranczyk, M., Algorithms and tools for high-throughput geometry-based analysis of crystalline porous materials. *Microporous Mesoporous Mater.* **2012,** *149* (1), 134-141.
37. Ongari, D.; Boyd, P. G.; Barthel, S.; Witman, M.; Haranczyk, M.; Smit, B., Accurate Characterization of the Pore Volume in Microporous Crystalline Materials. *Langmuir* **2017,** *33* (51), 14529-14538.
38. Guillerm, V.; Ragon, F.; Dan-Hardi, M.; Devic, T.; Vishnuvarthan, M.; Campo, B.; Vimont, A.; Clet, G.; Yang, Q.; Maurin, G.; Ferey, G.; Vittadini, A.; Gross, S.; Serre, C., A series of isoreticular, highly stable, porous zirconium oxide based metal-organic frameworks. *Angew. Chem. Int. Ed.* **2012,** *51* (37), 9267-9271.
39. Cavka, J. H.; Jakobsen, S.; Olsbye, U.; Guillou, N.; Lamberti, C.; Bordiga, S.; Lillerud, K. P., A new zirconium inorganic building brick forming metal organic frameworks with exceptional stability. *J. Am. Chem. Soc.* **2008,** *130* (42), 13850-13851.
40. Hu, Z.; Gami, A.; Wang, Y.; Zhao, D., A Triphasic Modulated Hydrothermal Approach for the Synthesis of Multivariate Metal-Organic Frameworks with Hydrophobic Moieties for Highly Efficient Moisture-Resistant CO2 Capture. *Adv. Sustainable Syst.* **2017,** *1* (11), 1700092.
41. Shannon, R. D., Revised effective ionic radii and systematic studies of interatomic distances in halides and chalcogenides. *Acta Crystallogr. A* **1976,** *32* (5), 751-767.
42. Hayes, S. A.; Yu, P.; O'Keefe, T. J.; O'Keefe, M. J.; Stoffer, J. O., The Phase Stability of Cerium Species in Aqueous Systems. *J. Electrochem. Soc.* **2002,** *149* (12), C623.
43. Estes, S. L.; Antonio, M. R.; Soderholm, L., Tetravalent Ce in the Nitrate-Decorated Hexanuclear Cluster [Ce6(μ3-O)4(μ3-OH)4]12+: A Structural End Point for Ceria Nanoparticles. *J. Phys. Chem. C* **2016,** *120* (10), 5810-5818.
44. Lanznaster, M.; Neves, A.; Bortoluzzi, A. J.; Assumpção, A. M. C.; Vencato, I.; Machado, S. P.; Drechsel, S. M., Electronic Effects of Electron-Donating and -Withdrawing Groups in Model Complexes for Iron-Tyrosine-Containing Metalloenzymes. *Inorg. Chem.* **2006,** *45* (3), 1005-1011.
45. Bêche, E.; Charvin, P.; Perarnau, D.; Abanades, S.; Flamant, G., Ce 3d XPS investigation of cerium oxides and mixed cerium oxide (CexTiyOz). *Surf. Interface Anal.* **2008,** *40* (3-4), 264-267.

46. Artiglia, L.; Orlando, F.; Roy, K.; Kopelent, R.; Safonova, O.; Nachtegaal, M.; Huthwelker, T.; van Bokhoven, J. A., Introducing Time Resolution to Detect Ce3+ Catalytically Active Sites at the Pt/CeO2 Interface through Ambient Pressure X-ray Photoelectron Spectroscopy. *J. Phys. Chem. Lett.* **2017,** *8* (1), 102-108.
47. Boudreaux, E. A.; Mulay, L. N., *Theory and Applications of Molecular Paramagnetism* Wiley-Interscience: New York, N.Y., 1976.
48. Walter, M. D.; Fandos, R.; Andersen, R. A., Synthesis and magnetic properties of cerium macrocyclic complexes with tetramethyldibenzotetraaza[14]annulene, tmtaaH2. *New J. Chem.* **2006,** *30* (7), 1065-1070.
49. Waitschat, S.; Fröhlich, D.; Reinsch, H.; Terraschke, H.; Lomachenko, K. A.; Lamberti, C.; Kummer, H.; Helling, T.; Baumgartner, M.; Henninger, S.; Stock, N., Synthesis of M-UiO-66 (M = Zr, Ce or Hf) employing 2,5-pyridinedicarboxylic acid as a linker: defect chemistry, framework hydrophilisation and sorption properties. *Dalton Transactions* **2018,** *47* (4), 1062-1070.
50. Buragohain, A.; Biswas, S., Cerium-based azide- and nitro-functionalized UiO-66 frameworks as turn-on fluorescent probes for the sensing of hydrogen sulphide. *CrystEngComm* **2016,** *18* (23), 4374-4381.
51. Sk, M.; Grzywa, M.; Volkmer, D.; Biswas, S., Zr(IV) and Ce(IV)-based metal-organic frameworks incorporating 4-carboxycinnamic acid as ligand: Synthesis and properties. *Microporous Mesoporous Mater.* **2017,** *237*, 275-281.
52. McDonald, T. M.; Mason, J. A.; Kong, X.; Bloch, E. D.; Gygi, D.; Dani, A.; Crocella, V.; Giordanino, F.; Odoh, S. O.; Drisdell, W. S.; Vlaisavljevich, B.; Dzubak, A. L.; Poloni, R.; Schnell, S. K.; Planas, N.; Lee, K.; Pascal, T.; Wan, L. F.; Prendergast, D.; Neaton, J. B.; Smit, B.; Kortright, J. B.; Gagliardi, L.; Bordiga, S.; Reimer, J. A.; Long, J. R., Cooperative insertion of CO2 in diamine-appended metal-organic frameworks. *Nature* **2015,** *519* (7543), 303-308.
53. Walton, K. S.; Millward, A. R.; Dubbeldam, D.; Frost, H.; Low, J. J.; Yaghi, O. M.; Snurr, R. Q., Understanding inflections and steps in carbon dioxide adsorption isotherms in metal-organic frameworks. *J. Am. Chem. Soc.* **2008,** *130* (2), 406-407.
54. Aguado, S.; Bergeret, G.; Titus, M. P.; Moizan, V.; Nieto-Draghi, C.; Bats, N.; Farrusseng, D., Guest-induced gate-opening of a zeolite imidazolate framework. *New J. Chem.* **2011,** *35* (3), 546-550.
55. Hyun, S. M.; Lee, J. H.; Jung, G. Y.; Kim, Y. K.; Kim, T. K.; Jeoung, S.; Kwak, S. K.; Moon, D.; Moon, H. R., Exploration of Gate-Opening and Breathing Phenomena in a Tailored Flexible Metal-Organic Framework. *Inorg. Chem.* **2016,** *55* (4), 1920-1925.
56. Liang, W.; Babarao, R.; Church, T. L.; D'Alessandro, D. M., Tuning the cavities of zirconium-based MIL-140 frameworks to modulate CO2 adsorption. *Chem. Commun.* **2015,** *51* (56), 11286-11289.
57. Lin, Y.; Kong, C.; Zhang, Q.; Chen, L., Metal-Organic Frameworks for Carbon Dioxide Capture and Methane Storage. *Adv. Energy Mater.* **2017,** *7* (4), 1601296.

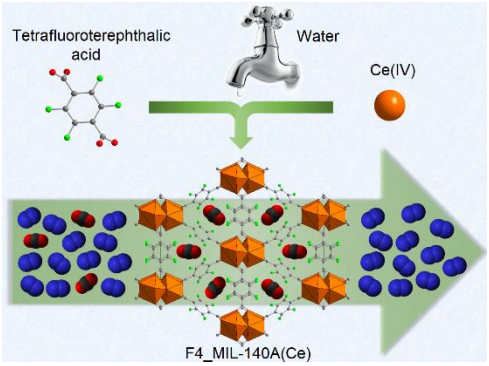
Tetrafluoroterephthalic acid
Water
Ce(IV)
F4_MIL-140A(Ce)